







## Article

# Electrodegradation of Acid Mixture Dye through the Employment Electrooxidation and *Lemnoideae* in Na<sub>2</sub>SO<sub>4</sub> Synthetic Wastewater

Agnieszka Bęś <sup>1</sup>, Łukasz Sikorski <sup>1</sup>, Tomasz Mikołajczyk <sup>1,\*</sup>, Mateusz Kuczyński <sup>1</sup>, Mateusz Łuba <sup>1</sup>,  
Bogusław Pierożyński <sup>1</sup> and Agnieszka Jasińska-Mikołajczyk <sup>2</sup>

<sup>1</sup> Department of Chemistry, Faculty of Agriculture and Forestry, University of Warmia and Mazury in Olsztyn, Łódzki Square 4, 10-727 Olsztyn, Poland

<sup>2</sup> Department of Pharmacology and Toxicology, Faculty of Veterinary Medicine, University of Warmia and Mazury in Olsztyn, Oczapowskiego 13, 10-719 Olsztyn, Poland

\* Correspondence: tomasz.mikolajczyk@uwm.edu.pl

**Abstract:** In this study, we report on the effectiveness of electrochemical and biological wastewater treatment for artificially prepared industrial wastewater, comprising small amounts of technologically important dyes, namely Acid Mixture composed of Acid Violet 90 (AV90) and Acid Red 357 (AR357) in Na<sub>2</sub>SO<sub>4</sub> (ESS—electrolyte supporting solution), as well as their impact on the environment, using *Lemna minor* as a bioindicator. Our study revealed that among the tested dyes, the raw ones (AM in ESS+OM) and those subjected to electrooxidation with the use of an iron anode and a copper cathode [AM<sub>Fe/CuOx</sub> in ESS+OM (OECD medium is a medium recommended by the Organization for Economic Co-operation and Development for *Lemna* sp. Growth Inhibition Test)] were the most phytotoxic for *L. minor*. No phytotoxicity was detected for the tested plants in solution after electrooxidation with graphite anode and cathode (AM<sub>Cox</sub> in ESS+OM). Quantitative identification of acid mixture removal was carried out by supplementary UPLC/MS-MS (Ultra-Performance Liquid Chromatography/tandem Mass Spectrometry) and UV-VIS (UltraViolet-Visible spectroscopy) instrumental analysis. The final removal after electrochemical and biological treatment of AV90 and AR357 dye components was 98 and over 99%, respectively. The results suggest that it may be a suitable replacement/addition for the generally used wastewater treatment methods.

**Keywords:** electrooxidation; galvanic cell; *Lemna minor*; wastewater treatment; acid mixture



**Citation:** Bęś, A.; Sikorski, L.; Mikołajczyk, T.; Kuczyński, M.; Łuba, M.; Pierożyński, B.; Jasińska-Mikołajczyk, A. Electrodegradation of Acid Mixture Dye through the Employment Electrooxidation and *Lemnoideae* in Na<sub>2</sub>SO<sub>4</sub> Synthetic Wastewater. *Appl. Sci.* **2022**, *12*, 8672. <https://doi.org/10.3390/app12178672>

Academic Editors: Wojciech Janczukowicz and Joanna Rodziewicz

Received: 25 July 2022

Accepted: 24 August 2022

Published: 29 August 2022

**Publisher's Note:** MDPI stays neutral with regard to jurisdictional claims in published maps and institutional affiliations.



**Copyright:** © 2022 by the authors. Licensee MDPI, Basel, Switzerland. This article is an open access article distributed under the terms and conditions of the Creative Commons Attribution (CC BY) license (<https://creativecommons.org/licenses/by/4.0/>).

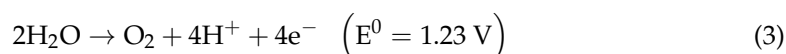
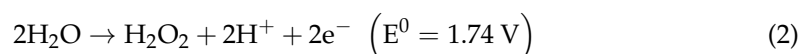
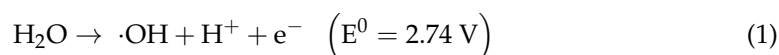
## 1. Introduction

The deficiency of fresh water has become a significant concern worldwide, as its quality and supply for domestic and industrial purposes are constantly deteriorating due to pollution. Numerous sources cause the above, including almost all industries, agricultural and mining activities, and municipal wastewater [1–3]. However, despite their well-documented hazardous effects on aquatic life and people, dyes are essential substrates in the textile, printing and food industries. The annual production of all commercially available dyes reaches a staggering amount of over 800,000 tons [4,5]. Among the various textile dyes, the most commonly used synthetic pigments are substances known as azo dyes, making up approximately 70% of the world's dye production. Azo dyes are characterized by the appearance of one or more azo group(s) (-N=N-) in their molecular structure [6–8].

Over the past several years, numerous attempts have been made to find the most suitable and safe methods for dye removal, including physical, chemical and biological techniques. Among these methods, biological processes are often favored due to their low impact on the environment and cost-effectiveness [9,10].

However, the high concentration of azo dyes and the presence of other chemicals (salts or surfactants) in the textile effluent repeatedly inhibited the process of azo dye biodegradation [1,9–12]. Hence, to improve the degradation of dyes, researchers have focused on

integrating biological treatment and advanced oxidation processes (AOPs) [9,13,14]. The characteristic feature of AOPs is the production of highly active radicals, which could be generated through a series of complex physical and chemical processes, including ozonation [15], photocatalysis [16], photo-Fenton [17] and electrochemical oxidation [18]. One of the most extensively researched AOPs is the electrochemical degradation technique due to its simplicity, fast reaction rate, and high oxidation efficiency. Additionally, it can mineralize the dye without the necessity of using additional chemicals [19]. Moreover, the operational cost can be reduced by employing a renewable energy source to power the process. The electrochemical oxidation of the pollutant can be proceed either by direct oxidation of the dye on the anode's surface or by the indirect oxidation caused by hydroxyl radicals ( $\cdot\text{OH}$ ) formed during the process. Such oxidant species are capable of oxidizing a wide variety of inorganic and organic pollutants [20,21]. However, the Faradic efficiency of  $\cdot\text{OH}$  production is inefficient compared to other more thermodynamically favorable water oxidation reactions occurring on the electrode-solution interface [22–26]. The above-mentioned reaction with their overpotential values is presented by Equations (1)–(3) below:



Nevertheless, most of the azo dyes are directly oxidized in lower potentials [27]; thus, electrodegradation methods are still a viable way to remove those pollutants. Moreover, electrochemical oxidation is characterized by the pollutant's rapid degradation rate (in the initial stage of the process), with decolorization efficiency ranging from 60 to over 90% depending on various conditions, such as current density or electrodes used [10,18,23,28,29].

Nonetheless, despite the high efficiency of such DC-powered systems, they still suffer from high electrical energy consumption, making them a relatively non-profitable method for dye removal. The above-mentioned issue could be resolved by applying an appropriately designed galvanic cell (cathode/anode) reactor. Employment of such a galvanic cell radically reduces total electricity consumption upon wastewater purification. An additional benefit of such a solution could be the process of electrocoagulation occurring when soluble metal ions (e.g.,  $\text{Fe}^{+2}$ ,  $\text{Al}^{+3}$ ) form insoluble hydroxide species, leading to precipitation of the pollutant [18,30]. However, the metal ions mentioned above could negatively influence biodegradation methods. Therefore, it is necessary to investigate the optimal option for dye removal.

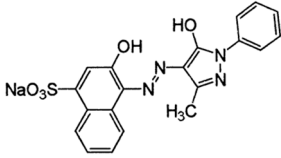
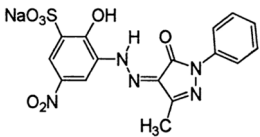
This study aimed to evaluate the effectiveness of combined methods of an initial anodic oxidation process and biological treatment of dye-based synthetic wastewater containing acid mixture (Acid Violet 90 and Acid Red 357). The *Lemna minor* was chosen as a biodegradation agent because it is applied as an indicator species in environmental risk analysis; thus, it could also be used to assess the toxicity of by-products that are formed during the electrolysis process. The decolorization and total dye removal of the acid mixture were investigated utilizing UV-VIS spectrophotometry analysis and ultra-performance liquid chromatography. The electrochemical oxidation process was done using two methods, one with and one without an external power supply. In the DC-powered method, the electrodes were made of graphite. The second process was based on earlier work from this laboratory [18] on the effectiveness of a Cu/Fe mild steel galvanic cell in the electrochemical treatment of analogous synthetic wastewater. Furthermore, the electrochemical parameters for the DC-controlled process were set up to easily compare the obtained results with those of the latter. Finally, the dye-based wastewater was treated with *L. minor* after both electrooxidation processes.

## 2. Materials and Methods

### 2.1. Chemicals and Solutions

The effectiveness of combined electrochemical and biological wastewater treatment methods was examined for industrially useful azo dyes, namely Acid Mixture (AM) (Acid Violet 90 and Acid Red 357; see its characteristics in Table 1, below) (P.A., Boruta-Zachem SA, Bydgoszcz, Poland). The initial mixture was composed of 0.054 M Na<sub>2</sub>SO<sub>4</sub>-based solution (P.A., Polish Chemical Compounds, Gliwice) with AM at a total concentration of 50 mg dm<sup>-3</sup>. To avoid spontaneous chemical coagulation, the pH of the working solution was adjusted to the set value of 3.05. Then, dilute sodium hydroxide (Sigma-Aldrich, Warsaw, Poland > 99%) and sulfuric acid solutions (Sigma-Aldrich, Warsaw, Poland > 99%) were employed to maintain the correct pH values during the electrolysis experiments. HCl solution was not used to avoid the possible chlorination effects of aromatic pollutants that could usually be present in industrial wastewater. Finally, to provide the required high efficiency of the surface electrooxidation processes, the conductivity of the working solutions was settled at about 15 mS.

Table 1. Specification of the dyes used in the research [31,32].

Chemical Compound	Structural Formula	Empirical Formula	CAS Number	Molecular Weight [g × mol <sup>-1</sup> ]
Acid Violet 90		C <sub>20</sub> H <sub>15</sub> N <sub>4</sub> NaO <sub>5</sub> S	6408-29-3	446.4
Acid Red 357		C <sub>16</sub> H <sub>12</sub> N <sub>5</sub> NaO <sub>7</sub> S	61951-36-8	441.4

### 2.2. Electrochemical Setup

The electrolysis unit used in this work consists of a single-compartment glass beaker (handle capacity of 500 cm<sup>3</sup>) with a bi-polar electrode setup. Cuboid-shaped graphite electrodes were used as both anode and cathode electrodes with an effective surface area of 74.56 cm<sup>2</sup> (HLM, Carbograf, Racibórz, Poland). In all the electrochemical experiments, the space between the electrodes was kept at about 3 cm. A saturated calomel electrode (SCE) was used as the reference electrode. All experiments were performed at room temperature. The Cu/Fe mild steel galvanic cell was set up according to Ref. [18]; also, to avoid repetition of the results, only the effect of the electrodegradation of this setup is discussed in this article.

Before the experiments, the graphite electrodes were first dipped in a 5% HCl solution to remove all the organic residuals from their surface. Then, the electrodes were submerged in acetone under ultra-sonication for 5 min before being rinsed with ultra-pure water (18.2 MΩ cm) from the Spring 30 s (Hydrolab, Straszyn, Poland) purification system.

All electrochemical experiments (CV and AC impedance spectroscopy tests) were performed using the AUTM204 + FRA32M Multi-Autolab potentiostat/galvanostat system (Metrohm Autolab B.V., Opacz-Kolonia, Poland). Otherwise, electrolyte pH and conductivity evaluations were carried-out with pHenomenal<sup>®</sup> pH 1100 L and pHenomenal<sup>®</sup> CO 3100 L meters from VWR (Gdańsk, Poland), correspondingly. The electrochemical impedance spectroscopy measurements were performed at an AC signal of 5 mV over the frequency range swept between 1.0 × 10<sup>5</sup> and 0.5 × 10<sup>-1</sup> Hz, whereas cyclic voltammetry (CV) experiments were performed at a sweep rate of 50 mV s<sup>-1</sup>. To perform all electrochemical experiments, the instruments were controlled by Nova 2.1 software for

Windows (Metrohm Autolab B.V., Opacz-Kolonia, Poland). Furthermore, all recorded cyclic voltammetry and impedance data were analyzed using the ZView 2.9 and Nova 2.3 software packages, respectively.

Electrochemical oxidation of the azo dyes in synthetic wastewater was considered the primary treatment process, with the following biological polishing. Initially, the one-hour electrolysis process was conducted in continuous galvanostatic mode, where the applied current density was at a level of  $0.29 \text{ mA cm}^{-2}$ . Then, about  $3 \text{ cm}^3$  of electrolytic solution was taken for UV-VIS analysis after 60 min of electrolysis.

### 2.3. Plant Material, Biological Treatment and Experimental Design

*L. minor* plants used in the research were a culture collection from the Department of Chemistry, University of Warmia and Mazury in Olsztyn, Poland.

After electrochemical treatment, the AM (dyes mixtures in the concentration of  $25 \text{ mg dm}^{-3}$ ) in the ESS ( $0.054 \text{ M Na}_2\text{SO}_4$ ) removal ability of *L. minor* was determined in Petri dishes filled with  $100 \text{ cm}^3$  of the following types of solution:

- OM-OECD medium;
- ESS+OM-electrolyte supporting solution: OECD medium, 1:1 (v/v);
- AM in ESS+OM-dyes mixtures in electrolyte supporting solution: OECD medium, 1:1 (v/v);
- $\text{AM}_{\text{Cox}}$  in ESS+OM-dyes mixtures in electrolyte supporting solution: OECD medium, 1:1 (v/v) after 1 h electrooxidation with graphite anode and cathode;
- $\text{AM}_{\text{Fe/Cuox}}$  in ESS+OM-dyes mixtures after 1 h electrooxidation in electrolyte supporting solution: OECD medium, 1:1 (v/v) after 1 h electrooxidation with iron anode and copper cathode.

The surface of the solutions was covered with plants 100%. The surface area of the Petri dishes in which the experiments were carried out was  $9326.59 \text{ mm}^2$  ( $\varnothing = 109 \text{ mm}$ ). The experiment began with an analysis of AM concentration.

The experiments lasted seven days and were independently replicated 6 times. During the experiment, the plants were kept under the same growth conditions described in section *L. minor*-growth inhibition test. After 7 days, the AM concentration was determined again.

*L. minor* was incubated for 7 days in 50 mL growth medium (OECD) for the testing of chemicals [33] in a floor standing incubator (ALL-Round-AI 185-4) illuminated with white fluorescent lighting ( $140 \mu\text{mol photon m}^{-2} \times \text{s}^{-1}$  PAR) in a light-to-dark cycle of 16 h/8 h (mean maximum temperature of  $20 \text{ }^\circ\text{C}$  in daytime and  $16 \text{ }^\circ\text{C}$  in night time). All solutions used for growth inhibition tests were prepared with deionized water (Adrona Water purification system Crystal 5 Basic, Riga, Latvia). Plants were exposed to OM, ESS+OM; AM in ESS+OM;  $\text{AM}_{\text{Cox}}$  in ESS+OM;  $\text{AM}_{\text{Fe/Cuox}}$  in ESS+OM. Figure 1 presents the scheme of the experiment's setup.

The assessment of the toxicity of all tested solutions was based on changes in the morphological features of *L. minor*: the percent inhibition of growth rate ( $I_r$ ), the percent reduction in yield ( $I_y$ ), the fresh mass of new fronds (FM) and dry matter content (DM). Leaf area measurement was determined using the Lucia 5.0 program (Laboratory Imaging, s.r.o., Prague, Czech Republic). The growth parameters  $I_r$  and  $I_y$  were determined based on the OECD guidelines, based on the number of *L. minor* fronds and frond area [33], using the following formulas:

$$\mu_{i-j} = [\ln(N_j) - \ln(N_i)]/t \quad (4)$$

$$I_r = (\mu_c - \mu_T)/\mu_c \times 100 \quad (5)$$

$$I_y = (b_c - b_T)/b_c \times 100 \quad (6)$$

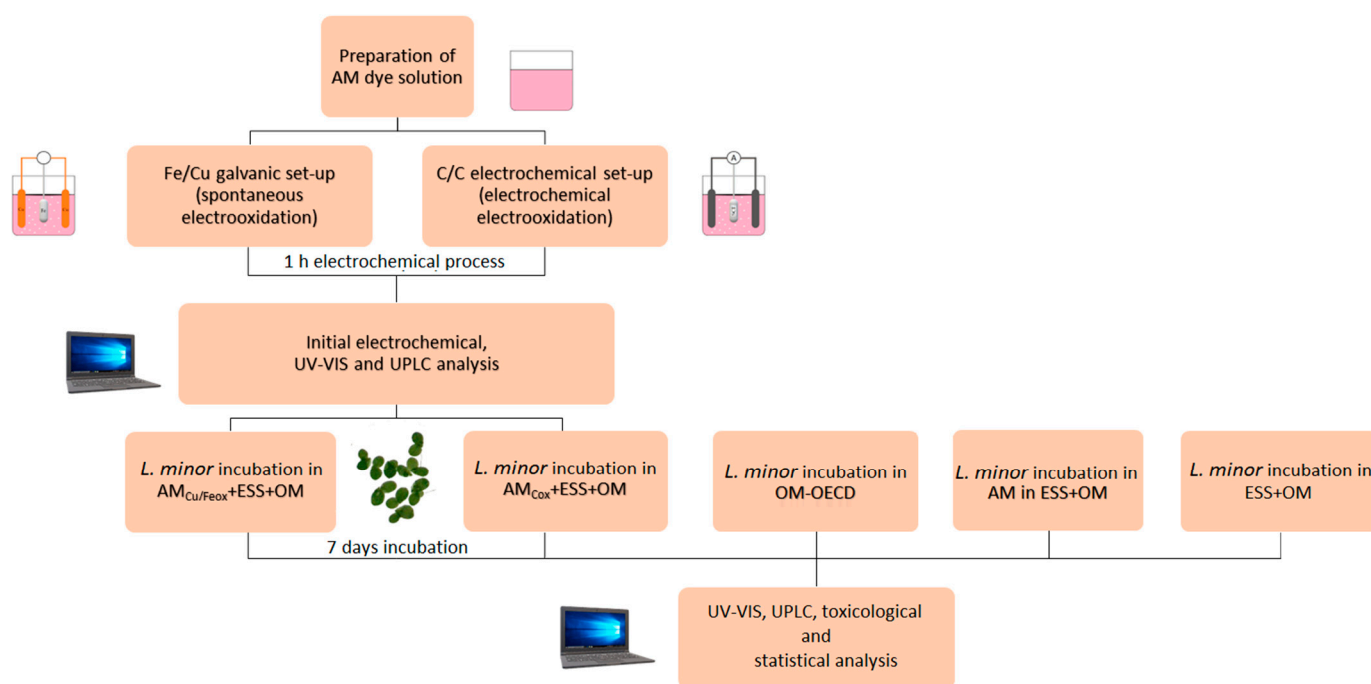
where:

$\mu_{i-j}$ —average specific growth rate from time i to j,

$N_i$ —measurement variable in the test or control vessel at time i,

$N_j$ —measurement variable in the test or control vessel at time j,

$t$ —time period from  $i$  to  $j$ ,  
 $\mu_c$ —mean value for  $\mu$  in the control,  
 $\mu_T$ —mean value for  $\mu$  in the treatment group,  
 $b_c$ —final number of *L. minor* fronds and frond area minus starting number of *L. minor* fronds and frond area for the control group,  
 $b_T$ —final number of *L. minor* fronds and frond area minus starting number of *L. minor* fronds and frond area in the treatment group.



**Figure 1.** Schematic diagram of the experimental setup.

#### 2.4. UV-VIS Spectroscopy Analysis

The efficiency evaluation of the wastewater purification treatment was determined using UV-VIS spectroscopic methods. The UV-VIS absorption spectra for the AM azo dye were recorded by means of the spectrophotometric plate reader EPOCH 2 (BIOTEK, Santa Clara, CA, USA) on polystyrene plates (UV-Star<sup>®</sup> Microplates, Greiner Bio One GmbH, Kremsmünster, Austria). The absorption spectra for all the collected samples were recorded for wavelengths between 230 and 999 nm. The results were then analyzed with Graph Pad Prism 6 software (Graph Pad, San Diego, CA, USA). The color removal's efficiency ( $\eta$ ) was calculated according to Equation (7) below (for the wavelength of 500 nm):

$$\eta = \frac{(c_0 - c_1)}{c_0} \cdot 100 \quad (7)$$

where:  $c_0$  is an initial dye concentration, and  $c_1$  is the dye concentration after one of the treatments.

#### 2.5. Chromatography Analysis

The chromatographic quantitation of AR357 and AV90 levels was achieved in a reversed-phase liquid chromatography ACQUITY UPLC (ultra-performance liquid chromatography) system with I-Class Plus coupled with an Xevo TQ-XS Triple Quadrupole Mass Spectrometry (Waters, Milford, CT, USA). The chromatographic separation of AR357 and AV90 dye components was performed using an ACQUITY UPLC BEH C18 column (1.7  $\mu\text{m}$ , 2.1  $\times$  50 mm, Waters) maintained at 50 °C. The mobile phase consisted of phase A (0.005% ammonium acetate for AR357 and AV90) and phase B (acetonitrile for AR357 and

AV90) in the gradient elution. Each sample analysis was carried out for 5 min at a flow rate of 400  $\mu\text{L min}^{-1}$ . The injection volume was 1  $\mu\text{L}$ , and the temperature of the autosampler was maintained at 15  $^{\circ}\text{C}$ . Detection was performed with a double quadrupole tandem mass spectrometer in negative ion mode for both AR357 and AV90 pigments. The setting parameters of the detector are illustrated in Table 2 below. Equipment was set up in multiple reaction monitoring (MRM) mode, and transitions of 447.5 and 442.5  $m/z$  were used to determine the AR357 and AV90 parts, respectively. Samples collected from electrolysis (100  $\mu\text{L}$  of AM) were dissolved in water to achieve a final volume of 500  $\mu\text{L}$  and transferred into full recovery vials (Waters). Finally, an aliquot was injected for UPLC-MS/MS analysis.

**Table 2.** Tandem mass spectrometry (MS/MS) parameters.

MS/MS Parameters	
Precursor ion ( $m/z$ )	447.5 (AR357) 442.5 (AV90)
Product ions ( $m/z$ )	-
Desolvation gas	nitrogen
Desolvation gas temperature ( $^{\circ}\text{C}$ )	350
Desolvation gas flow (L/h)	300
Cone gas flow (L/h)	150
Collision gas	argon
Source's temperature ( $^{\circ}\text{C}$ )	120
Electrospray mode	negative
Cone voltage (V)	20
Capillary voltage (kV)	3.0
Retention time (min)	0.89 (AV90) 1.10 (AR357)

## 2.6. Statistical Analysis

Six replicates were conducted in the experiment. The results are presented as the mean  $\pm$  standard deviation (SD). The results were statistically compiled using ANOVA (F test) for one factor—the solution type used (to Ir, Iy, FM and DM) (Table 3). Tukey's test was used to determine significant differences at  $p < 0.01$ . The research results were performed using the STATISTICA 13.3 statistical package (TIBCO Software Inc., Palo Alto, USA, 2018). The assessment of the toxicity was based on the number and total area, FM and DM of fronds [33–35].

**Table 3.** Analysis of variance (ANOVA) for morphological features of *L. minor* exposed to OM, ESS+OM; AM in ESS+OM; AM<sub>Cox</sub> in ESS+OM; AM<sub>Fe/Cuox</sub> in ESS+OM.

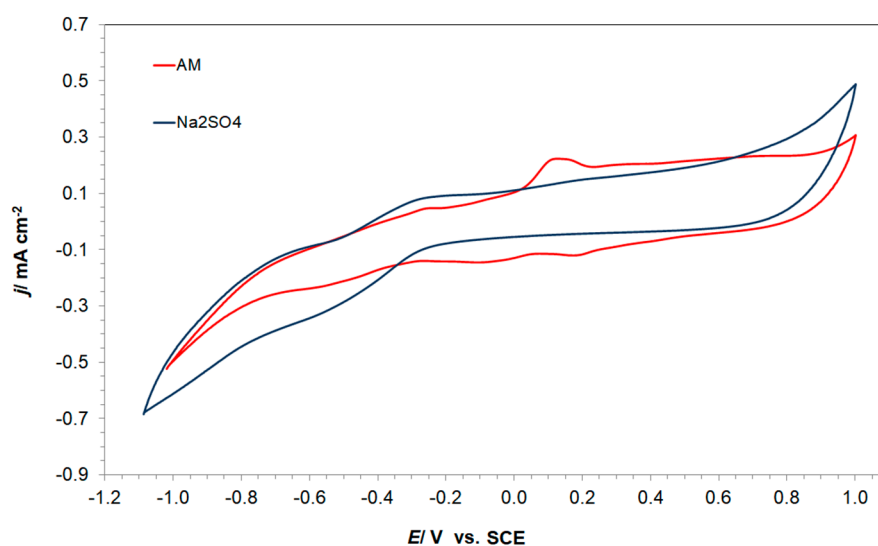
Source of Variation	Ir		Iy		FM		DM	
	F-Value	p	F-Value	p	F-Value	p	F-Value	p
Intercept	63.10554 *	0.000000	82.17460 *	0.000000	442.0006 *	0.000000	781.8951	0.000000
Solution type (S)	25.82239 *	0.000000	19.27117 *	0.000000	37.3908 *	0.000005	1.5545	0.259981

S—solution type, \* significant at  $p < 0.01$ .

## 3. Results

### 3.1. Electrochemistry

Before conducting the electrodegradation of the azo dye, cyclic voltammetry (CV) and AC impedance methods were employed to examine the electrochemical behavior of graphite electrodes in pure and AM-modified 0.054 M  $\text{Na}_2\text{SO}_4$  solutions. Figure 2 shows the cyclic voltammograms recorded for both solutions over the potential range from  $-1.00$  to  $1.00$  V vs. SCE, obtained at room temperature with a sweep rate of  $50 \text{ mV s}^{-1}$ .



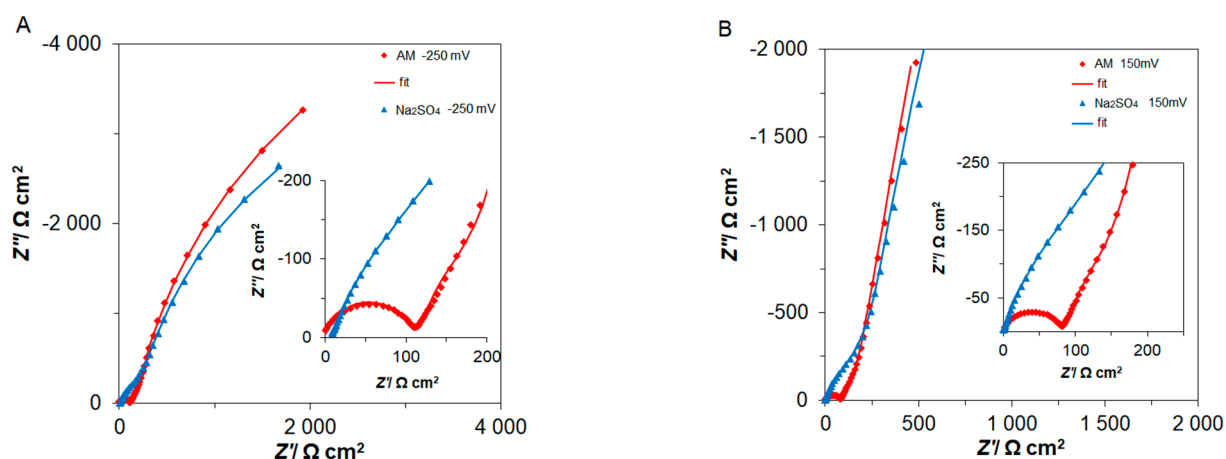
**Figure 2.** Cyclic voltammetry behavior of the graphite electrode in the absence and presence of AM dye (at  $50 \text{ mg dm}^{-3}$ ), recorded in  $0.054 \text{ M Na}_2\text{SO}_4$  supporting electrolyte, at a sweep rate of  $50 \text{ mV s}^{-1}$  and  $293 \text{ K}$ .

The voltammogram in pure solution exhibited well-defined cathodic and anodic features related to Faradaic hydrogen and oxygen evolution reactions in the potential range from  $-1.10$  to  $-0.30 \text{ V}$  and from  $0.60$  to  $1.00 \text{ V}$  vs. SCE, respectively. The rest of the CV profile could be associated with a double-layer charging process.

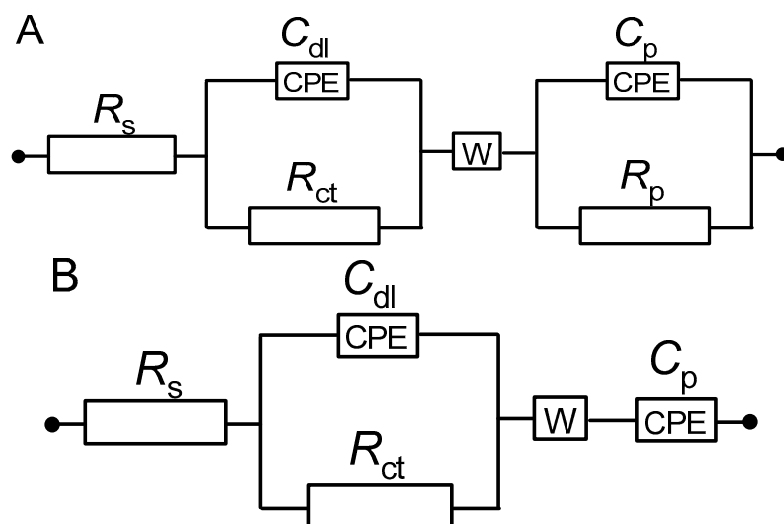
Then, the addition of AM dye caused the appearance of two well-pronounced oxidation peaks (centered at about  $-0.25$  and  $0.10 \text{ V}$  vs. SCE) upon cycling in the direction of more positive potentials reaching current densities of  $0.05$  and  $0.22 \text{ mA cm}^{-2}$ , correspondingly. It is strongly believed that they are related to the surface oxidation of the studied dyes [36,37]. Later, another two features were observed on the reverse scan, located from  $0.10$  to  $0.25$  and from  $-0.20$  to  $0.05$ . These peaks are most presumably associated with the reduction of earlier electrooxidized by-products.

A similar CV response was observed for the Fe working electrode of the Cu/Fe galvanic cell, where two oxidation peaks were also obtained under analogous conditions [18]. Nevertheless, they were centered in more negative regions than those for graphite electrodes and were centered at ca.  $-0.56$  and  $-0.42 \text{ V}$  vs. SEC. They were also characterized by higher current densities than those obtained in this work, namely  $2.0$  and  $3.8 \text{ mA cm}^{-2}$ . The above may suggest that iron has better catalytic properties than graphite for AM electrooxidation.

The electrochemical spectroscopy impedance (EIS) behavior of the graphite electrode in pure and containing  $50 \text{ mg dm}^{-3}$  of AM dye supporting a  $0.054 \text{ M Na}_2\text{SO}_4$  solution is shown in Figure 3A,B (the potentials of EIS measurements correspond to potentials of oxidation peaks from Figure 2). Hence, in the absence of the AM dye (Figure 3A) for the applied potential of  $-250 \text{ mV}$  vs. SCE, the Nyquist impedance plot (blue) exhibited two somewhat “depressed” semicircles, where it is strongly believed that the high-frequency and low-frequency semicircles were associated with the porosity of the electrode [38]. In the presence of the AM dye for the same potential, the features observed in the Nyquist impedance plot (red) corresponded to the initial phase of the dye electrooxidation (for high-frequency arc), while middle-frequency and low-frequency features could be assigned to finite-length diffusion related to surface porosity [18,38]. Thus, for the first oxidation peak (Figure 2), the recorded charge transfer resistance ( $R_{ct}$ ) parameter for AM oxidation came to  $108 \Omega \text{ cm}^2$ , whereas the recorded porosity resistance ( $R_p$ ) of the electrode’s surface reached  $11,636 \Omega \text{ cm}^2$ . Moreover, the corresponding interfacial capacitance ( $C_{dl}$ ) and pseudocapacitance ( $C_p$ ) parameters reached  $2.21$  and  $1535 \mu\text{F cm}^{-2}$ , respectively (see equivalent circuits used to fit the recorded data in Figure 4A).



**Figure 3.** The recorded complex plane Nyquist impedance plots for a graphite electrode in contact with pure  $\text{Na}_2\text{SO}_4$  and AM-modified ( $50 \text{ mg dm}^{-3}$ ) solution, where (A) corresponds to the potential of  $-250 \text{ mV}$  vs. SCE and (B) corresponds to the potential of  $150 \text{ mV}$  vs. SCE. The solid lines correspond to the data representation according to the equivalent circuit model presented in Figure 4.



**Figure 4.** Equivalent circuit models used for fitting the obtained AC impedance spectroscopy data, where  $R_s$  is solution resistance;  $C_{dl}$  is double-layer capacitance;  $R_{ct}$  is charge-transfer resistance parameter for electrooxidation AM dye molecule;  $W$  is Warburg element used to account for finite-length diffusion; (A)  $R_p$  and  $C_p$  are porosity resistance and pseudocapacitance parameters, respectively; (B)  $C_p$  is the pseudocapacitance parameter. In addition, the circuits include constant phase elements (CPEs) to account for the distributed capacitance.

Then, only porosity response was observed in a pure supporting solution at the potential of  $150 \text{ mV}$  vs. SCE (Figure 3B, blue plot). On the other hand, in the AM-containing solution (red) for the same potential (corresponding to the second oxidation peak, see Figure 2), a high-frequency semicircle appeared, which could be associated with the process of dye electrooxidation. At the same time, middle-frequency and low-frequency features can be assigned to diffusion and porosity phenomena. Here, the  $R_{ct}$  parameter came to  $74 \Omega \text{ cm}^2$ , and the  $C_{dl}$  and  $C_p$  parameter reached  $4.04$  and  $2218 \mu\text{F cm}^{-2}$  (see equivalent circuits used to fit the recorded data in Figure 4B).

Thus, the  $R_{ct}$  parameter corresponding to the oxidative electrodegradation of the dye components diminished by about 30% for the peak potential points. The above reactivity increase aligns with the noted augmentation of recorded capacitance parameters by  $1.8\times$  and  $0.7\times$ , correspondingly for  $C_{dl}$  and  $C_p$ . The above also aligns with previously obtained results in Fe/Cu galvanic cell [18]. The  $R_{ct}$  parameter's decrease is associated with the

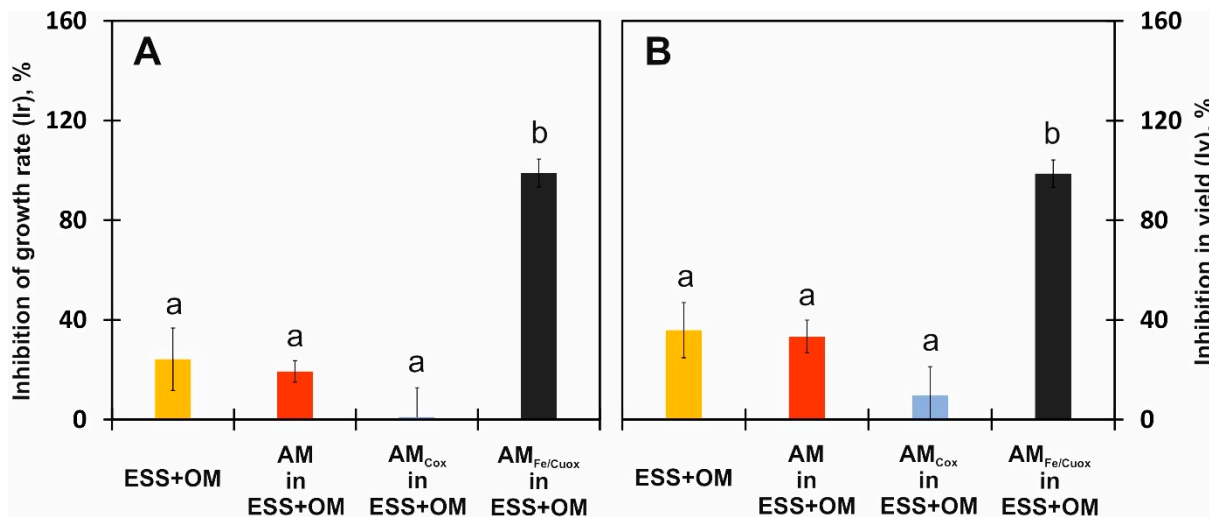


facilitation of the oxidation process with rising potential, whereas the augmentation of the capacitance values could be associated with the adsorption of oxidation's products on the surface of the electrode.

Alternatively, the EIS results for the pure  $\text{Na}_2\text{SO}_4$  solution were omitted, as they did not provide any insights into the process of electrooxidation of the examined dye at the investigated potentials. Therefore, they were presented only in graphs to show the difference in the EIS response between pure and AM-modified supporting solutions.

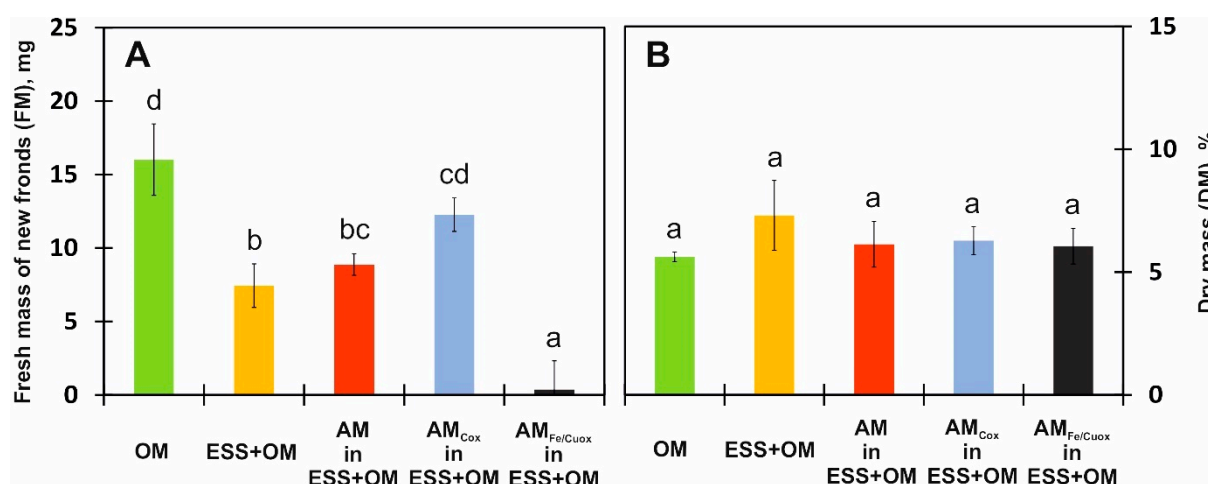
### 3.2. Growth Rate, Biomass Yield of *Lemna minor*

This study evaluated the effects of ESS+OM; AM in ESS+OM;  $\text{AM}_{\text{Cox}}$  in ESS+OM;  $\text{AM}_{\text{Fe/Cuox}}$  in ESS+OM (AM in concentration  $25 \text{ mg dm}^{-3}$ ) and on Ir, Iy, FM and DM content and the results were compared with the OM-OECD (control sample). After 7 days of incubation, growth parameters were calculated from the number and area of *L. minor* leaves. The experiment demonstrated that solution type modified the Ir, Iy and FM of *L. minor*. The addition of an electrolyte supporting solution (ESS) to the medium (OM) caused the growth rate of *L. minor* to decrease by 24% compared to the control sample (OM), but it was not statistically significant. Meanwhile, the sample containing the dyes (AM in ESS+OM) was slightly less toxic for the tested plants, with no significant Ir = 19% growth inhibition. No phytotoxicity (Ir = 0.28%) was observed in the solution after electrooxidation using graphite electrodes ( $\text{AM}_{\text{Cox}}$  in ESS+OM). On the other hand, *L. minor* placed in the mixture of dyes subjected to electrooxidation conducted by means of the Fe/Cu galvanic cell ( $\text{AM}_{\text{Fe/Cuox}}$  in ESS+OM) did not grow at all; its Ir increased significantly to 99% (Figure 5A). A similar trend as in Ir was also noted for Iy. Iy in mixtures of ESS+OM; AM in ESS+OM;  $\text{AM}_{\text{Cox}}$  in ESS+OM and  $\text{AM}_{\text{Fe/Cuox}}$  in ESS+OM was 36, 34, 9 and 99% respectively (Figure 5B).



**Figure 5.** Inhibition of growth rate (Ir) (A) and inhibition in yield (Iy) (B) of *L. minor* exposed to OM, ESS+OM; AM in ESS+OM;  $\text{AM}_{\text{Cox}}$  in ESS+OM;  $\text{AM}_{\text{Fe/Cuox}}$  in ESS+OM. The data points represent the mean  $\pm$  SD,  $n = 6$ . Values are significantly different from the control at  $p < 0.01$  (a, b).

The FM of *L. minor* new fronds was found to be highest (16 mg) in OM. Among the samples contaminated with dyes, the highest FM = 12.27 mg was recorded in  $\text{AM}_{\text{Cox}}$  in ESS+OM (statistically not different from the control sample), while no new leaves appeared in  $\text{AM}_{\text{Fe/Cuox}}$  in ESS+OM (0.37 mg); FM did not increase. At the same time, the FM of *L. minor* growing in AM in ESS+OM was 8.88 mg, and the one exposed to ESS+OM—7.44 mg (Figure 6A).



**Figure 6.** Fresh mass (FM) (A) of new fronds, dry matter content (DM) (B) of *L. minor* exposed to OM, ESS+OM; AM<sub>in</sub> ESS+OM; AM<sub>in</sub> ESS+OM<sub>Cox</sub>; AM<sub>in</sub> ESS+OM<sub>Fe/Cuox</sub>. The data points represent the mean  $\pm$  SD, n = 6. Values are significantly different from the control at  $p < 0.01$  (a–d).

The dry matter content (DM) of the control plants (OM) was 5.62% on average. Plants growing in ESS+OM had 7.31% DM, while the DM of those exposed to AM<sub>in</sub> ESS+OM; AM<sub>in</sub> ESS+OM<sub>Cox</sub>; AM<sub>in</sub> ESS+OM<sub>Fe/Cuox</sub> had an average value of 6.15% (Figure 6B).

According to the OECD [33] and ISO [34] recommendations, the toxicity of xenobiotic toxicity can rely on evaluating the morphological features of *Lemma* sp. This study examined the exposure effects of the *L. minor* on the dyes Acid Violet 90 and Acid Red 357 in an Acid Mixture before and after using two electrooxidation types. Thus, the samples containing 25 mg dm<sup>-3</sup> the dye (AM<sub>in</sub> ESS+OM), which were not subjected to electrooxidation, had 19% growth inhibition (Ir). However, when the dyes were subjected to electrooxidation using graphite electrodes (AM<sub>in</sub> ESS+OM<sub>Cox</sub>), no phytotoxicity of these dyes was noted. (Figure 4A,B). The phytotoxicity of xenobiotics is defined as the lowest applied concentration (LOEC) of a chemical compound, reducing the measured response by more than 20% [39]. Already, a small amount of gentian violet and Congo red not electro-oxidized decreases the values of Ir and Iy by 20% already in the concentration of 0.10 and 0.64 mg dm<sup>-3</sup>, respectively [40]. Dyes show different phytotoxicity. A high concentration (40 mg dm<sup>-3</sup>) of malachite green (triarylmethane dye) high (in 77%) inhibits the relative growth rate and the number of leaves (in 85%) of *L. minor* [41], while methylene blue inhibits the growth of the same plants by 46.52% [42]. Not only the type of dye but also the influence of physicochemical pretreatments applied to it affect the toxicity of dyes. During the process of electrooxidation, the iron ions are released from the electrode to the medium. These ions can be phytotoxic. Water plants *S. polyrrhiza* (L.) Schleid after 24 h treatments of 100 mg dm<sup>-3</sup> Fe accumulated 6.84 mg g<sup>-1</sup> of these ions in the DW. Due to accumulation, it has been observed that fronds are dark brown and necrotic or dead [43]. Iron oxide nanoparticles are also highly toxic to aquatic plants. According to the authors, iron oxide in concentrations  $\geq 30$  mg dm<sup>-3</sup> kills *L. minor* within 7 days. The authors also report that lipid peroxidation in the tissues increased with increasing iron oxide nanoparticles concentration, the chlorophyll content decreased at 50 mg dm<sup>-3</sup> of iron oxide nanoparticles and Fe<sup>3+</sup> accumulation in *L. minor* roots, which can inhibit nutrient uptake [44]. In this study, the mixture of dyes (25 mg dm<sup>-3</sup>) was subjected to electrooxidation with the use of an iron anode and a copper cathode (AM<sub>in</sub> ESS+OM<sub>Fe/Cuox</sub>) was lethal for *L. minor* (Figure 4A,B). The same effect (Ir = 100%) causes 12 mg dm<sup>-3</sup> of gentian violet—an aniline-derived triphenylmethane dye [45,46]. Congo red—a benzidine-derived azo dye in the same concentration, inhibits plant growth by half (Ir = 50%) [40]. Plant growth inhibition results in a reduction in FM (total wet weight) of *L. minor*. The reduction in FM due to exposure to Direct Red 28 was reported by Lobiuc et al. [47], under the influence of

gentian violet and Congo red [40]. In addition, the tested dyes decreased the FM (total wet weight) of *L. minor*.

Xenobiotics in high concentrations in water manifest in the form of hypertonic and hyperosmotic stress, which results in dehydration of *L. minor* tissues and an increase in DM [48]. When the osmotic pressure in plants decreases, they are unable to take up the water, which results in stomata closing and a drop in turgor pressure. The dyes caused membrane disintegration, dehydration of tissues, and a systematic increase in DM, which reached an average of 6.15% in plants exposed to AC (AM in ESS+OM; AM<sub>Cox</sub> in ESS+OM; AM<sub>Fe/Cuox</sub> in ESS+OM). Meanwhile, DM in the control plants (OM) was determined to be 5.62% (Figure 6B). However, when the FM of common wheat seedlings (*Triticum aestivum*) decreased in a study by Shivangi and Kumar [49], then the textile dyes had no effect on DM.

These findings imply that among the studied samples, the untreated (AM in ESS+OM) and those subjected to electrooxidation with the use of an iron anode and a copper cathode (AM<sub>Fe/Cuox</sub> in ESS+OM) were the most phytotoxic for *L. minor* and the least were those where electrooxidation was carried out using graphite electrodes (AM<sub>Cox</sub> in ESS+OM). High concentrations of raw malachite green [50] and Brilliant Blue R [51] were also the cause of the strongly reduced growth of *L. minor*. Raw Congo red at a concentration of 2500 ppm totally inhibited the growth of *L. minor* [47]. Nevertheless, the inhibition of plant morphological features is a secondary toxicity effect of xenobiotics. Yaseen et al. [52] also observed that the growth rate was an indirect marker of dyes' toxicity to *L. minor*. It is concluded that xenobiotics also decrease the FM of plants, inhibit the chlorophyll biosynthesis pathway [53–55] and limit photosynthesis, thus reducing the yield. Hence, the supposition is that the inhibition of the plant growth rate is the result of chlorophyll degradation at the photosynthetic apparatus level. In the present study, the leaves exposed to the dyes were not green, as the pigments were transferred to the tissues (Table 4). Dyes in the *L. minor* tissues affected chlorophyll content. Adomas et al. [39] reported that after 7 days of biotest, the high content (12.5 mg L<sup>-1</sup>) of gentian violet and Congo red in medium decreased Chl *a* in tissues by 65 and 29%, respectively. Also, Congo red at concentrations higher than 2500 ppm limits the content of Chl *a* in the tissues of *L. minor* [47]. Likewise, a reduction in the content of assimilation pigments was noted in *L. minor* exposed to crystal violet and malachite green [50] *L. minor* tissues retained absorbed pigments, and the dye disturbed light from reaching the photosynthetic reaction centre [40].

### 3.3. Dye Removal Assessment


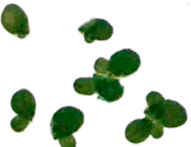



As the electrochemical decomposition characteristics and analysis of the by-products of the AM dye were already extensively described in previous work from this laboratory [18], this article will focus on the quantitative evaluation of AM dye removal methods. The efficiency of the electrooxidation and biodegradation processes of the examined AM azo dye for different experimental setups was evidenced by utilizing UV-Vis spectrophotometry and UPLC-MS/MS analysis (see Table 5 and Table 6, respectively).

Hence, based on UV-Vis spectrophotometry results (Table 5), the total quantitative removal of the AM dye after 1h of continuous electrolysis yielded ca. 35 and 40% for AM<sub>Cox</sub> in ESS+OM and AM<sub>Fe/Cuox</sub> in ESS+OM conditions, respectively. This is in line with the electrochemical results, which suggest that the Fe electrode could possess superior catalytic properties toward AM dye oxidation compared to the graphite electrode. Then, after 7 days of exposure to the *L. minor*, the total removal of the researched dyes came to about 49, 63 and 68% for AM in ESS+OM, AM<sub>Cox</sub> in ESS+OM and AM<sub>Fe/Cuox</sub> in ESS+OM solutions, correspondingly. The above shows that *L. minor*'s outstanding removal ability of AM dye could be further enhanced by applying pretreatment, such as electrooxidation.

A similar trend of the AM dye's removal was evidenced by UPLC-MS/MS analysis (see Table 6). Nevertheless, compared with the UV-Vis spectrophotometry method, the degree of AM dye removal registered by UPLC-MS/MS analysis was significantly higher. The above most likely results from the selectivity discrepancy between these two analytical

methods. Then, the final removal of AV90 and AR357 dye components was 98 and over 99%, respectively, for both AM<sub>Cox</sub> in ESS+OM and AM<sub>Fe/Cuox</sub> in ESS+OM solutions.

**Table 4.** The leaves of *L. minor* were exposed to OM, ESS+OM; AM in ESS+OM; AM<sub>Cox</sub> in ESS+OM; AM<sub>Fe/Cuox</sub> in ESS+OM.

Solution	Visible Symptoms
OM	
ESS+OM	
AM in ESS+OM	
AM <sub>Cox</sub> in ESS+OM	
AM <sub>Fe/Cuox</sub> in ESS+OM	

**Table 5.** Quantitative dye assay was recorded for a wavelength of 500 nm.

Sample	Concentration of Dye (mg dm <sup>-3</sup> )	Decrease in the Dye Concentration (%) (Total)
AM in ESS+OM (before incubation)	23.057	-
AM in ESS+OM (after incubation)	11.803	49
AM <sub>Cox</sub> in ESS+OM (before incubation)	14.921	35
AM <sub>Cox</sub> in ESS+OM (after incubation)	8.451	43 (63)
AM <sub>Fe/Cuox</sub> in ESS+OM (before incubation)	13.653	40
AM <sub>Fe/Cuox</sub> in ESS+OM (after incubation)	7.466	45 (68)

**Table 6.** Variation of the detected chromatographic peak areas for AV90 and AR357 substrate components for different removal treatments.

Sample	Peak Area	
	AV90	AR357
AM in ESS+OM (before incubation)	614,605	116,270
AM in ESS+OM (after incubation)	55,637	1918
AM <sub>Cox</sub> in ESS+OM (before incubation)	58,070	2205
AM <sub>Cox</sub> in ESS+OM (after incubation)	12,269	93
AM <sub>Fe/Cuox</sub> in ESS+OM (before incubation)	47,203	1516
AM <sub>Fe/Cuox</sub> in ESS+OM (after incubation)	10,112	120

**Table 7.** Comparison of various novel azo dyes removal methods.

Method of Azo Dyes Removal	Type of Process	Total Removal %	Exposure Time	Use of External Power Supply	Current Density (mA cm <sup>-2</sup> )	Use of Toxic Chemicals	Ref.
AM in ESS+OM	Biological	48%	7 days	No	-	No	This work
AM <sub>Cox</sub> in ESS+OM	Combination of chemical and biological methods	63%	1 h + 7 days (Electrochemical + biological techniques)	Yes	0.29	No	This work
AM <sub>Fe/Cuox</sub> in ESS+OM	Combination of physico-chemical and biological methods	68%	1 h + 7 days (Electrochemical + biological techniques)	No	0.29	No	This work
<i>L. minor</i>	Biological	98%	14 days	No	-	No	[50]
Novel yeast consortium	Biological	6–16%	1 h	No	-	Heavy metals	[36]
Electrochemical degradation with BDD-anode	Physico-chemical	ca. 40%	1 h	Yes	30.00	No	[23]
<i>L. minor</i>	Biological	ca. 39%	7 days	No	-	No	[47]
Tank with <i>Chlorella vulgaris</i> microalgae	Biological	ca. 18%	2 days	No	-	No	[56]
Electrochemical treatment with Aluminum anodes	Physico-chemical	87%	1 h	Yes	-	Yes (Cl <sub>2</sub> formation)	[57]
Electrochemical treatment with Sb-doped SnO <sub>2</sub> ceramic electrodes	Physico-chemical	ca. 50%	1 h	Yes	15.00	No	[19]

Furthermore, Table 7 presents the efficiencies of other azo dyes' degradation methods described in the literature. It should be noted that direct comparison of efficiencies with literature is quite problematic, as even similar methods have different starting and final conditions, such as time of the experiment and applied current densities, amount of used plants or starting dye concentration. Nevertheless, after considering all the conditions, the techniques employed in this work could be considered promising alternatives or additions to commonly used degradation methods.

#### 4. Conclusions

This study's proposed wastewater treatment method was based on electrochemical and biological arrangements. The results suggest that it may be a suitable replacement/addition for the generally used wastewater treatment methods. Nevertheless, the selection of an appropriate pretreatment method (electrooxidation) for such an application needs to consider not only the highest and cheapest solutions but also their impact on the environment; thus, *L. minor* was employed in this work, as it is an important bioindicator used to assess the toxicity of chemical compounds. However, published data about electrooxidized dyes' influence on *L. minor* growth are still lacking.

According to the OECD and ISO recommendations, toxicity assessment should be based on the morphological parameters of the plants. Our study revealed that among the tested dyes, the raw ones (AM in ESS+OM) and those subjected to electrooxidation with the use of an iron anode and a copper cathode (AM<sub>Fe/CuOx</sub> in ESS+OM) were the most phytotoxic for *L. minor*. No phytotoxicity was detected for the tested plants in AM<sub>CoX</sub> in ESS+OM solution. The above proved that even a method with slightly worse performance in dye removal and the need to use an external power supply is more suitable as an effective method for removing the tested dyes.

**Author Contributions:** Conceptualization, T.M. and Ł.S.; methodology, T.M. and Ł.S.; investigation, M.K., M.Ł. and A.J.-M.; data curation, M.K., M.Ł., A.J.-M. and A.B.; writing—original draft preparation, Ł.S., T.M., A.B. and B.P.; writing—review and editing, T.M. and Ł.S.; supervision, B.P. All authors have read and agreed to the published version of the manuscript.

**Funding:** This project was financially supported by the Minister of Education and Science under the program entitled "Regional Initiative of Excellence" for the years 2019–2022, Project No. 010/RID/2018/19, amount of funding 12.000.000 PLN. The results in this paper were obtained as part of a comprehensive study financed by the University of Warmia and Mazury in Olsztyn, Faculty of Agriculture and Forestry, Department of Chemistry (grant no. 30.610.001-110 and 30.610.002-110). The project was also supported by grant no. 15.610.008-110, provided by the University of Warmia and Mazury in Olsztyn.

**Institutional Review Board Statement:** Not applicable.

**Informed Consent Statement:** Not applicable.

**Data Availability Statement:** The data presented in this study are available on request from the corresponding author.

**Acknowledgments:** Mateusz Łuba would like to acknowledge a scholarship from the program Interdisciplinary Doctoral Studies in Bioeconomy (POWR.03.02.00-00-1034/16-00), funded by the European Social Fund.

**Conflicts of Interest:** The authors declare no conflict of interest.

#### References

1. Jamee, R.; Siddique, R. Biodegradation of Synthetic Dyes of Textile Effluent by Microorganisms: An Environmentally and Economically Sustainable Approach. *Eur. J. Microbiol. Immunol.* **2019**, *9*, 114–118. [[CrossRef](#)]
2. Zamora-Ledezma, C.; Negrete-Bolagay, D.; Figueroa, F.; Zamora-Ledezma, E.; Ni, M.; Alexis, F.; Guerrero, V.H. Heavy Metal Water Pollution: A Fresh Look about Hazards, Novel and Conventional Remediation Methods. *Environ. Technol. Innov.* **2021**, *22*, 101504. [[CrossRef](#)]
3. Hadi Hassan Al-Taai, S. Ground Water: A Study of Its Importance, Its Sources, and the Causes of Its Pollution. *Mater. Today Proc.* **2021**. [[CrossRef](#)]
4. Hassaan, M.A.; Nembr, A.E. Health and Environmental Impacts of Dyes: Mini Review. *Am. J. Environ. Sci. Eng.* **2017**, *1*, 64–67. [[CrossRef](#)]
5. Yusuf, M. Synthetic Dyes: A Threat to the Environment and Water Ecosystem. In *Textiles and Clothing*; Shabbir, M., Ed.; Wiley: Hoboken, NJ, USA, 2019; pp. 11–26. ISBN 978-1-119-52631-5.
6. Benkhaya, S.; M'rabet, S.; El Harfi, A. Classifications, Properties, Recent Synthesis and Applications of Azo Dyes. *Heliyon* **2020**, *6*, e03271. [[CrossRef](#)] [[PubMed](#)]
7. Rawat, D.; Sharma, R.S.; Karmakar, S.; Arora, L.S.; Mishra, V. Ecotoxic Potential of a Presumably Non-Toxic Azo Dye. *Ecotoxicol. Environ. Saf.* **2018**, *148*, 528–537. [[CrossRef](#)]

8. Valica, M.; Hostin, S. Electrochemical Treatment of Water Contaminated with Methylorange. *Nova Biotechnol. Chim.* **2016**, *15*, 55–64. [[CrossRef](#)]
9. Sathishkumar, K.; AlSalhi, M.S.; Sanganyado, E.; Devanesan, S.; Arulprakash, A.; Rajasekar, A. Sequential Electrochemical Oxidation and Bio-Treatment of the Azo Dye Congo Red and Textile Effluent. *J. Photochem. Photobiol. B* **2019**, *200*, 111655. [[CrossRef](#)]
10. Crini, G.; Lichtfouse, E. Advantages and Disadvantages of Techniques Used for Wastewater Treatment. *Environ. Chem. Lett.* **2019**, *17*, 145–155. [[CrossRef](#)]
11. Sharma, S.; Saxena, R.; Gaur, G.; Gaur, G. Study of Removal Techniques for Azo Dyes by Biosorption: A Review. *IOSR J. Appl. Chem.* **2014**, *7*, 06–21. [[CrossRef](#)]
12. Singh, P.K.; Singh, R.L. Bio-Removal of Azo Dyes: A Review. *Int. J. Appl. Sci. Biotechnol.* **2017**, *5*, 108–126. [[CrossRef](#)]
13. Advanced Oxidation Processes for Waste Water Treatment. In *Emerging Green Chemical Technology*; Ameta, S.C., Ameta, R., Eds.; Academic Press: Cambridge, MA, USA, 2018; pp. 1–412, ISBN 978-0-12-810499-6.
14. Liu, L.; Chen, Z.; Zhang, J.; Shan, D.; Wu, Y.; Bai, L.; Wang, B. Treatment of Industrial Dye Wastewater and Pharmaceutical Residue Wastewater by Advanced Oxidation Processes and Its Combination with Nanocatalysts: A Review. *J. Water Process Eng.* **2021**, *42*, 102122. [[CrossRef](#)]
15. Li, P.; Miao, R.; Wang, P.; Sun, F.; Li, X. Bi-Metal Oxide-Modified Flat-Sheet Ceramic Membranes for Catalytic Ozonation of Organic Pollutants in Wastewater Treatment. *Chem. Eng. J.* **2021**, *426*, 131263. [[CrossRef](#)]
16. Mahendran, V.; Gogate, P.R. Degradation of Acid Scarlet 3R Dye Using Oxidation Strategies Involving Photocatalysis Based on Fe Doped TiO<sub>2</sub> Photocatalyst, Ultrasound and Hydrogen Peroxide. *Sep. Purif. Technol.* **2021**, *274*, 119011. [[CrossRef](#)]
17. Kuntail, J.; Verma, A.; Kumar, S.; Sinha, I. Photo-Fenton Interfacial Phenomena on Graphene Oxide: Computational and Experimental Investigations. *J. Mol. Liq.* **2021**, *342*, 117461. [[CrossRef](#)]
18. Kuczyński, M.; Łuba, M.; Mikołajczyk, T.; Pierożyński, B.; Jasiocka-Mikołajczyk, A.; Smoczyński, L.; Sołowiej, P.; Wojtacha, P. Electrodegradation of Acid Mixture Dye through the Employment of Cu/Fe Macro-Corrosion Galvanic Cell in Na<sub>2</sub>SO<sub>4</sub> Synthetic Wastewater. *Molecules* **2021**, *26*, 4580. [[CrossRef](#)]
19. Droguett, T.; Mora-Gómez, J.; García-Gabaldón, M.; Ortega, E.; Mestre, S.; Cifuentes, G.; Pérez-Herranz, V. Electrochemical Degradation of Reactive Black 5 Using Two-Different Reactor Configuration. *Sci. Rep.* **2020**, *10*, 4482. [[CrossRef](#)]
20. Henke, A.H.; Saunders, T.P.; Pedersen, J.A.; Hamers, R.J. Enhancing Electrochemical Efficiency of Hydroxyl Radical Formation on Diamond Electrodes by Functionalization with Hydrophobic Monolayers. *Langmuir* **2019**, *35*, 2153–2163. [[CrossRef](#)]
21. Moreira, F.C.; Boaventura, R.A.R.; Brillas, E.; Vilar, V.J.P. Electrochemical Advanced Oxidation Processes: A Review on Their Application to Synthetic and Real Wastewaters. *Appl. Catal. B Environ.* **2017**, *202*, 217–261. [[CrossRef](#)]
22. Chen, M.; Ding, W.; Wang, J.; Diao, G. Removal of Azo Dyes from Water by Combined Techniques of Adsorption, Desorption, and Electrolysis Based on a Supramolecular Sorbent. *Ind. Eng. Chem. Res.* **2013**, *52*, 2403–2411. [[CrossRef](#)]
23. Brito, C.N.; Ferreira, M.B.; de Moura Santos, E.C.M.; Léon, J.J.L.; Ganiyu, S.O.; Martínez-Huitle, C.A. Electrochemical Degradation of Azo-Dye Acid Violet 7 Using BDD Anode: Effect of Flow Reactor Configuration on Cell Hydrodynamics and Dye Removal Efficiency. *J. Appl. Electrochem.* **2018**, *48*, 1321–1330. [[CrossRef](#)]
24. García-Osorio, D.A.; Jaimes, R.; Vazquez-Arenas, J.; Lara, R.H.; Alvarez-Ramirez, J. The Kinetic Parameters of the Oxygen Evolution Reaction (OER) Calculated on Inactive Anodes via EIS Transfer Functions: ·OH Formation. *J. Electrochem. Soc.* **2017**, *164*, E3321. [[CrossRef](#)]
25. Wang, C.; Tong, H.; Lu, J.; Liu, B.; Zheng, F.; Tao, W.; Zhang, W.; Chen, Q. Boosting Oxygen Evolution Reaction on Graphene through Engineering Electronic Structure. *Carbon* **2020**, *170*, 414–420. [[CrossRef](#)]
26. Borah, M.; Sikdar, A.; Kapse, S.; Majumdar, A.; Dutta, P.; Karim, G.M.; Deb, S.; Thapa, R.; Maiti, U.N. Stable and Boosted Oxygen Evolution Efficiency of Mixed Metal Oxide and Borate Planner Heterostructure over Heteroatom (N) Doped Electrochemically Exfoliated Graphite Foam. *Catal. Today* **2021**, *370*, 83–92. [[CrossRef](#)]
27. Costa, M.C.; Mota, F.S.B.; Santos, A.B.D.; Mendonça, G.L.F.; Nascimento, R.F.d. Effect of Dye Structure and Redox Mediators on Anaerobic Azo and Anthraquinone Dye Reduction. *Quím. Nova* **2012**, *35*, 482–486. [[CrossRef](#)]
28. Yaseen, D.A.; Scholz, M. Textile Dye Wastewater Characteristics and Constituents of Synthetic Effluents: A Critical Review. *Int. J. Environ. Sci. Technol.* **2019**, *16*, 1193–1226. [[CrossRef](#)]
29. de Oliveira, G.A.R.; Leme, D.M.; de Lapuente, J.; Brito, L.B.; Porredón, C.; de Brito Rodrigues, L.; Brull, N.; Serret, J.T.; Borràs, M.; Disner, G.R.; et al. A Test Battery for Assessing the Ecotoxic Effects of Textile Dyes. *Chem. Biol. Interact.* **2018**, *291*, 171–179. [[CrossRef](#)]
30. Łuba, M.; Mikołajczyk, T.; Pierożyński, B.; Smoczyński, L.; Wojtacha, P.; Kuczyński, M. Electrochemical Degradation of Industrial Dyes in Wastewater through the Dissolution of Aluminum Sacrificial Anode of Cu/Al Macro-Corrosion Galvanic Cell. *Molecules* **2020**, *25*, 4108. [[CrossRef](#)]
31. CAS 6408-29-3 PubChem, Compound Summary for CID 136496748, Acid Violet 90. Available online: <https://pubchem.ncbi.nlm.nih.gov/compound/136496748> (accessed on 26 March 2021).
32. CAS 61951-36-8 PubChem, Compound Summary for CID 137270279, Acid Red 357. Available online: <https://pubchem.ncbi.nlm.nih.gov/compound/137270279> (accessed on 26 March 2021).

33. OECD. *Guideline for Testing of Chemicals, Section 2 Test No.221: Lemna Sp. Growth Inhibition Test*; Organisation for Economic Co-Operation and Development: Paris, France, 2006; Available online: <https://www.oecd-ilibrary.org/docserver/9789264016194-en.pdf?expires=1661779910&id=id&accname=guest&checksum=ED22427A4C657941254AA4333FC74E4D> (accessed on 26 March 2021).
34. ISO 20079: 2005; Water Quality—Determination of Toxic Effect of Water Constituents and Wastewater on Duckweed (Lemna Minor)—Duckweed Growth Inhibition Test. The International Organization for Standardization: Geneva, Switzerland, 2005.
35. EPA Ecological Effects Test Guidelines. OCSPP: 850.4400: Aquatic Plant Toxicity Test Using Lemna Spp. U.S. EPA 712-C-008. United States Environmental Protection Agency. 2012. Available online: <https://nepis.epa.gov/Exe/tiff2png.cgi/P100IR97.PNG?-r+75+-g+7+D%3A%5CZYFILES%5CINDEX%20DATA%5C11THRU15%5CTIFF%5C00000670%5CP100IR97.TIF> (accessed on 26 March 2021).
36. Ali, S.S.; Al-Tohamy, R.; Koutra, E.; Kornaros, M.; Khalil, M.; Elsamahy, T.; El-Shetehy, M.; Sun, J. Coupling Azo Dye Degradation and Biodiesel Production by Manganese-Dependent Peroxidase Producing Oleaginous Yeasts Isolated from Wood-Feeding Termite Gut Symbionts. *Biotechnol. Biofuels* **2021**, *14*, 61. [[CrossRef](#)]
37. Nie, C.; Dong, J.; Sun, P.; Yan, C.; Wu, H.; Wang, B. An Efficient Strategy for Full Mineralization of an Azo Dye in Wastewater: A Synergistic Combination of Solar Thermo- and Electrochemistry plus Photocatalysis. *RSC Adv.* **2017**, *7*, 36246–36255. [[CrossRef](#)]
38. Lasia, A. *Electrochemical Impedance Spectroscopy and Its Applications*; Springer: New York, NY, USA, 2014; ISBN 978-1-4614-8932-0.
39. Efroymson, R.; Will, M.; Suter, G., II; Wooten, A. *Toxicological Benchmarks for Screening Contaminations of Potential Concern for Effects on Terrestrial Plants: 1997 Revision*; U.S. Department of Energy: Washington, DC, USA, 1997.
40. Adomas, B.; Sikorski, L.; Beś, A.; Warmiński, K. Exposure of Lemna Minor L. to Gentian Violet or Congo Red Is Associated with Changes in the Biosynthesis Pathway of Biogenic Amines. *Chemosphere* **2020**, *254*, 126752. [[CrossRef](#)] [[PubMed](#)]
41. Torbati, S. Feasibility and Assessment of the Phytoremediation Potential of Duckweed for Triarylmethane Dye Degradation with the Emphasis on Some Physiological Responses and Effect of Operational Parameters. *Turk. J. Biol.* **2015**, *39*, 438–446. [[CrossRef](#)]
42. Imron, M.F.; Kurniawan, S.B.; Soegianto, A.; Wahyudianto, F.E. Phytoremediation of Methylene Blue Using Duckweed (Lemna Minor). *Heliyon* **2019**, *5*, e02206. [[CrossRef](#)] [[PubMed](#)]
43. Xing, W.; Huang, W.; Liu, G. Effect of Excess Iron and Copper on Physiology of Aquatic Plant Spirodela Polyrhiza (L.) Schleid. *Environ. Toxicol.* **2010**, *25*, 103–112. [[CrossRef](#)] [[PubMed](#)]
44. Souza, L.R.R.; Bernardes, L.E.; Barbeta, M.F.S.; da Veiga, M.A.M.S. Iron Oxide Nanoparticle Phytotoxicity to the Aquatic Plant Lemna Minor: Effect on Reactive Oxygen Species (ROS) Production and Chlorophyll a/Chlorophyll b Ratio. *Environ. Sci. Pollut. Res.* **2019**, *26*, 24121–24131. [[CrossRef](#)]
45. CAS 573-58-0 PubChem, Compound Summary for CID 11313, Congo Red. Available online: <https://pubchem.ncbi.nlm.nih.gov/compound/11313> (accessed on 26 March 2021).
46. CAS 548-62-9 PubChem, Compound Summary for CID 11057, Gentian-Violet. Available online: <https://pubchem.ncbi.nlm.nih.gov/compound/11057> (accessed on 26 March 2021).
47. Lobiuc, A.; Olaru, S.; Olaru, E.-I.; Zamfirache, M.; Naela, C.; Fortuna, M.; Constantinescu, G. Toxicity and Removal of Direct Red 28 Diazo Dye in Living Polymeric Systems. *Rev. Chim. Buchar. Orig. Ed.* **2018**, *69*, 1628. [[CrossRef](#)]
48. Baciak, M.; Sikorski, L.; Piotrowicz-Cieślak, A.; Adomas, B. Content of Biogenic Amines in Lemna Minor (Common Duckweed) Growing in Medium Contaminated with Tetracycline. *Aquat. Toxicol.* **2016**, *180*, 95–102. [[CrossRef](#)]
49. Rana, S.; Kumar, K. Study of Phytotoxic Effect of Textile Wastewater on Seed Germination and Seedling Growth of Triticum Aestivum. *Int. J. Biosci. Technol.* **2017**, *10*, 58–66.
50. Török, A.; Buta, E.; Indolean, C.; Tonk, S.; Silaghi-Dumitrescu, L.; Majdik, C. Biological Removal of Triphenylmethane Dyes from Aqueous Solution by Lemna Minor. *Acta Chim. Slov.* **2015**, *62*, 452–461. [[CrossRef](#)]
51. Cleuvers, M.; Ratte, H.T. The Importance of Light Intensity in Algal Tests with Coloured Substances. *Water Res.* **2002**, *36*, 2173–2178. [[CrossRef](#)]
52. Yaseen, D.; Scholz, M.; Clausner, C.; Antonacopoulos, A. Assessing the Impact of Dyes Accumulation on the Growth of Lemna Minor L. Using Image Processing Technique. In *Proceeding of CSE 2017 Annual PGR Symposium (CSE-PGSym17) 17th March 2017*; The University of Salford: Salford, UK, 2017.
53. Sikorski, L.; Adomas, B.; Dobiesz, M.; Baciak, M.; Piotrowicz-Cieślak, A. Morphological and Biochemical Responses of Lemna Minor L. (Common Duckweed) to Ciprofloxacin. *Fresenius Environ. Bull.* **2014**, *23*, 363–371.
54. Pokharia, A.; Singh, S. Toxicological Effect of Textile Dyes and Their Metabolites: A Review Current Trends in Biotechnology and Chemical Research. *Curr. Trends Biotechnol. Chem. Res.* **2015**, *5*, 11–17.
55. Bradel, B.G.; Preil, W.; Jeske, H. Remission of the Free-Branching Pattern of Euphorbia Pulcherrima by Tetracycline Treatment. *J. Phytopathol.* **2000**, *148*, 587–590. [[CrossRef](#)]
56. Ishchi, T.; Sibi, G. Azo Dye Degradation by Chlorella Vulgaris: Optimization and Kinetics. *Int. J. Biol. Chem.* **2019**, *14*, 1–7. [[CrossRef](#)]
57. Palanisamy, S.; Nachimuthu, P.; Awasthi, M.K.; Ravindran, B.; Chang, S.W.; Palanichamy, M.; Nguyen, D.D. Application of Electrochemical Treatment for the Removal of Triazine Dye Using Aluminium Electrodes. *J. Water Supply Res. Technol. Aqua* **2020**, *69*, 345–354. [[CrossRef](#)]